Numerical parametric study for different cold storage designs and strategies of a solar driven thermoacoustic cooler system

Maxime Perier-Muzet, P Stouffs, Jean-Pierre Bedecarrats, Jean Castaing-Lasvignottes

Numerical parametric study for different cold storage designs and strategies of a solar driven thermoacoustic cooler system

Maxime Perier-Muzet[a], Pascal Stouffs[b], Jean-Pierre Bedecarrats[c] and Jean Castaing-Lasvignottes[d]

[a] *Université de Pau et des Pays de l'Adour, LaTEP, Pau, France, maxime.perier-muzet@etud.univ-pau.fr* ***(CA)***
[b] *Université de Pau et des Pays de l'Adour, LaTEP, Pau, France, pascal.stouffs@univ-pau.fr*
[c] *Université de Pau et des Pays de l'Adour, LaTEP, Pau, France, jean-pierre.bedecarrats@univ-pau.fr*
[d] *Laboratoire de Physique Et Ingénierie Mathématique pour l'Energie et l'environnemeNT (PIMENT), Ile de la Réunion, France, jean.castaing-lasvignottes@univ-reunion.fr*

Abstract:

A heat driven thermoacoustic cooler consists of a thermoacoustic engine that converts heat into acoustic waves, coupled to a thermoacoustic cooler that converts this acoustic energy into cooling effect. These machines have simple structures without moving parts. The coupling of a solar concentrator and a heat driven thermoacoustic cooler seems to be an interesting alternative to the electrically driven compression vapour cycle. As the other solar refrigeration systems, even if the cooling demand generally increases with the intensity of the solar radiation, one of the major difficulties is to insure a frigorific power supply when there is no or low solar radiation. In our prototype, in order to guarantee a sufficient cooling capacity to face to refrigeration loads in spite of the production fluctuations, a latent cold storage has been considered. The aim of the work presented here is to investigate the behaviour of this key element under several design and operative conditions. A description of the future prototype is done insisting on the thermoacoustic refrigeration and the cold storage system. A modelling of the main elements of the prototype is developed. The results of simulations under real solar radiation as well as a parametric study considering the main design and operative parameters of the cold thermal storage system are presented.

Keywords:

Solar energy, Solar refrigeration, Thermoacoustic refrigerator, Cold latent thermal storage.

1. Introduction

Energy use for refrigeration has risen sharply in recent years. Nowadays, the major part of this production is provided by electrically driven vapour compression machines. Globally, the refrigeration devices consumed roughly 15% of the world electricity production. The forecasts for the refrigeration indicate an increase in the number of units in operation over the coming years. To ensure the refrigerating production in the next years while responding to environmental challenges (emissions of greenhouse gases and ozone layer) the future cooling machines should not be primary energy intensive and should use environmentally friendly refrigerants [1, 2].

Thanks to numerous possible combinations between solar thermal collectors and heat driven cooling machines, solar cooling equipment seems to be an interesting alternative [3]. Among these possibilities, the coupling of a solar concentrator with a heat driven thermoacoustic refrigerator is a promising technology. Compared to the other refrigeration technologies, heat driven thermoacoustic machines have several advantages with no moving part and environmentally friendly gas as working fluid like helium, argon or air [4]. During the last decades, experimental investigations have been carried out on these machines. They have proven their ability to reach very low temperatures compatible with the liquefaction of gases such as, natural gas, nitrogen or hydrogen [5-7]. Other studies have demonstrated the possibility to uses thermoacoustic refrigeration for higher temperature applications like for food refrigeration [8]. The couplings of thermodriven

thermoacoustic refrigerators and solar concentrators have also already been experimentally studied thanks to low power prototypes [9, 10].

Although the cooling demand is generally higher when the sun is shining, the intermittent nature of solar energy is one of the major constraints for using solar cooling systems. To meet the time-dependency of the primary energy supply and end-use requirement, a thermal energy storage has to be used. Various configurations of the energy storage can be achieved; storing the hot energy for continuously supply the refrigeration system or storing the produced cool energy. This energy can be stored in the form of sensible heat (in liquid or in solid), latent heat of a Phase Change Material (PCM), or by chemical reaction. The choice of the storage system depends on various criteria like the amount of energy that has to be stored or the storage temperature. However for cooling application, the latent storages have numerous advantages: the technology is well known with a high energy storage density; the stored and retrieved energy is at a quasi constant temperature which corresponds to the phase change transition of the PCM [11].

The studied prototype consists in a one kW scale solar thermodriven thermoacoustic refrigerator supplied in primary energy by a solar dish concentrator. To ensure a low variability of the availability of refrigerating capacity, a cold latent thermal storage is coupled to the refrigerator.

In the first part of this paper the project and the main parts of its development are presented. Secondly, the lumped model that has been built is described. Then, the first simulation results for a long period including days with various solar radiation conditions are presented and discussed. Finally, the results of the parametric study are presented, considering the above-mentioned different cold storage design characteristics and storage strategies.

2. Prototype description

The device considered here consists in a solar concentrator, a solar flux modulator, a solar receiver, a thermoacoustic machine composed firstly of a thermoacoustic prime mover linked to an acoustic resonator and secondly of a thermoacoustic refrigerator linked to a cool thermal energy storage (Fig. 1).

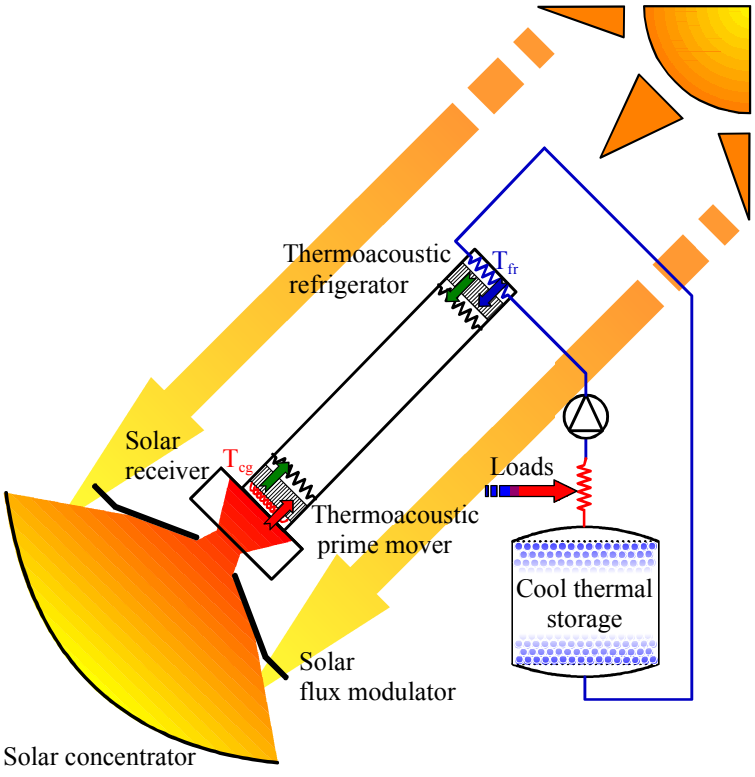

Fig. 1. Solar driven thermoacoustic refrigerator experimental plant

The solar driven thermoacoustic refrigerator heat fluxes represented in Fig. 2 are described in the following sections. The direct solar radiation is collected, reflected and concentrated by a parabolic mirror. More details on this element can be found in [12]. A solar flux modulator is placed between the concentrator and the receiver cavity. This element regulates the solar power entering in the absorbing cavity; it thus allows controlling the temperature of this latter. The concentrated solar radiation is collected by an absorber situated in the receiver cavity. This latter transfers approximately 4 kW to the working fluid (helium at about 4 MPa), while being at a temperature close to 500°C. More details on this component can be found in [13, 14].

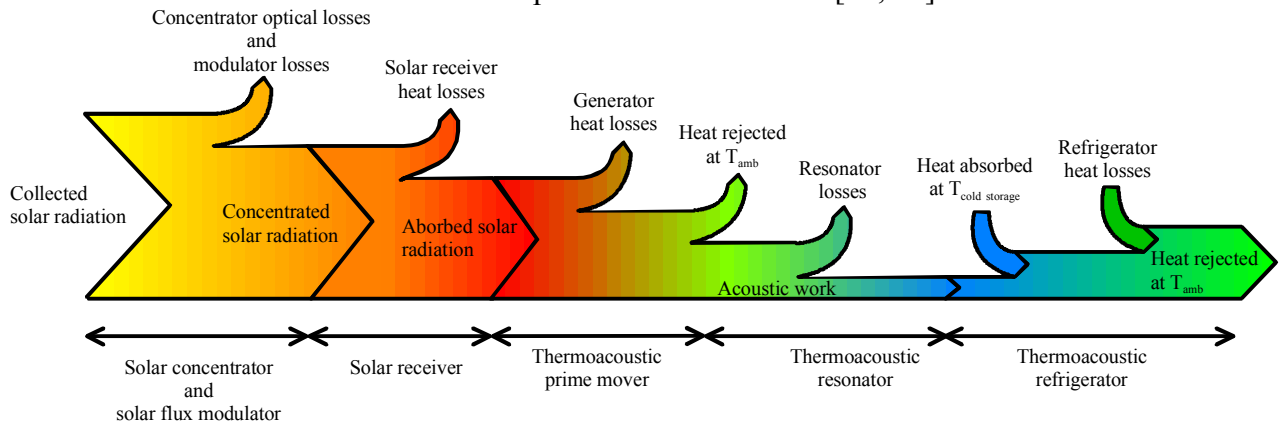

Fig. 2. Solar driven thermoacoustic refrigerator heat fluxes

The thermoacoustic cooler is composed of a wave generator, an acoustic resonator and a thermoacoustic refrigerator. Thank to the solar heat absorbed, the thermoacoustic prime mover generates a traveling wave with large acoustic power. This power is used into the thermoacoustic refrigerator to pump approximately 800 W of heat from the cold heat exchanger and reject it at the intermediate temperature exchanger of the refrigerator. A detailed explanation of the way these coolers work is given in [15].

To ensure a constant power supply at the cold exchanger, a latent storage is intended to be used. This later uses encapsulated nodules filled with an eutectic Phase Change Material (PCM). The storage tank is filled with these nodules and the cold transfer fluid which circulates in the tank ensures the heat exchange between the PCM and the cold production unit [16]. During the time where the tank is being cooled, the crystallization of nodules allows the storage of the energy.

To produce a controlled thermal load, an electrical fluid circulation heater is placed between the storage tank and the cold heat exchanger. The power regulation of this latter allows generating different consumption and storage strategies.

3. Modelling

To predict the future performance of the prototype a lumped model of the entire plant has been developed. The time variation of the energy source and the frigorific power consumption imposes a transient approach. The solar part and the cold storage are treated by simplified transient models. For the thermodriven thermoacoustic refrigerator, a quasi-stationary approach it used. We describe the equations and the principal assumptions of this model in the following sections.

3.1. The solar concentrator and the solar flux modulator

The solar concentrator consists in a 8.5 m diameter parabolic mirror. For this prototype, the aperture of the dish is reduced at 13.5 m² by using non reflective bands at the concentrator periphery. Thanks to the sun tracking system, solar rays are always perpendicular to the collector aperture. The collecting solar power is calculated as following:

$$\dot{Q}_{sol\_collect} = A_{collector\_aperture} . DNI \,, \qquad (1)$$

Where *DNI* is the Direct Normal Irradiation and $A_{collector\_aperture}$ is the collector aperture area.

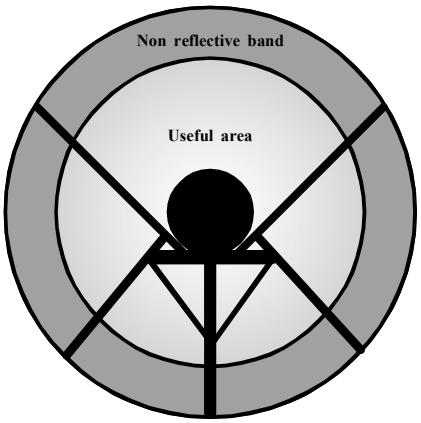

Fig. 3. Concentrator aperture

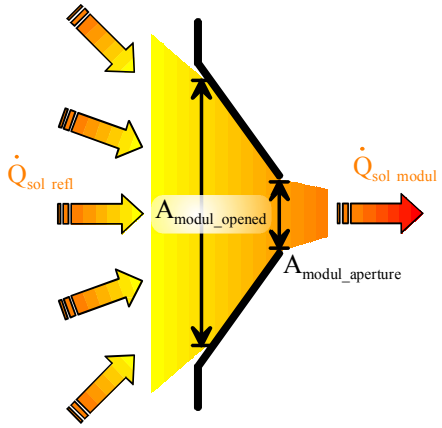

Fig. 4. Modulator geometry

The Thermoacoustic machine, the flow pipes, the frame of the concentrator, etc… shadow a part of the dish (Fig. 3). The sun tracking system is considered to be accurate so that the useful area of the concentrator remains constant all along the day. A constant and uniform mirror reflectivity is assumed. According these hypotheses, the reflected solar power is expressed by:

$$\dot{Q}_{sol\_reflect} = A_{collector\_useful} \cdot \chi . DNI \,, \qquad (2)$$

Where $A_{collector\_useful}$ is the useful area of the concentrator aperture calculated by $A_{collector\_useful} = A_{collector\_aperture} - A_{shadow}$, and χ is the mirror reflectivity.

A uniform solar concentrated flux is assumed in the modulator plan (Fig. 4). It is also considered that it has no impact if it is totally opened. The solar modulated power is determined by:

$$\dot{Q}_{sol\_modul} = \dot{Q}_{sol\_reflect} \frac{A_{modul\_aperture}}{A_{modul\_opened}} \,, \qquad (3)$$

Where $A_{modul\_aperture}$ is the area of the modulator aperture and A_{modul_opened} is the area of the modulator aperture when it is totally opened.

3.2. The solar driven thermoacoustic refrigerator

We consider in this modelling, a uniform wall and fluid temperature in all heat exchangers of the thermoacoustic device. The temperature of the hot exchanger of the thermoacoustic generator is also assumed to be equal to the temperature of the solar receiver cavity wall.

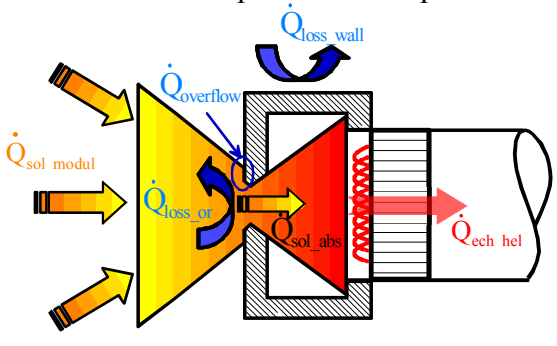

Fig. 5. Absorber cavity and hot exchanger heat fluxes

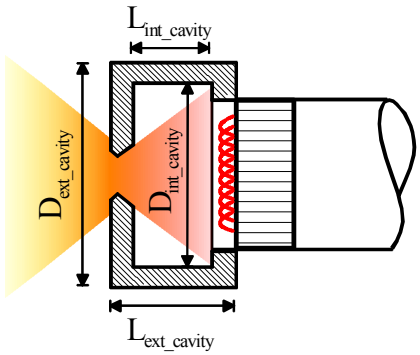

Fig. 6. Absorber cavity geometry

The cavity absorbs the solar concentrated flux. Thanks to the hot exchanger, a large part of this heat flux is transferred to the working fluid, the rest is exchanged with the surroundings (Fig. 5). The

cavity walls are considered as an equivalent mass of the hot exchanger. The energy balance of these elements can be written as:

$$\frac{dU_{cavity+hg}}{dt} = \dot{Q}_{sol\_abs} + \dot{Q}_{loss\_cavity} + \dot{Q}_{hel-wall\_hg}, \qquad (4)$$

Where $\dot{Q}_{sol\_abs}$ is the absorbed solar power. The absorber cavity absorbs the major part of the solar power which passes through the solar flux modulator. The rest is the solar loss by overflow. This loss is due to the diameter difference between the solar focus point and the cavity orifice. If the diameter of the focal point is larger than the one of the cavity aperture (as it is the case for the studied prototype, in order to limit the thermal losses through the orifice) a part of the solar radiation cannot enter in this later. In this model, the solar overflow losses are evaluated considering a solar overflow rate ($\tau_{sol\_overflow}$). This rate is equal to a constant value when the solar flux modulator is totally opened and equal to zero when the modulator is partially closed. The absorbed solar power is calculated by:

$$\dot{Q}_{sol\_abs} = \dot{Q}_{sol\_modul} \cdot \left(1 - \tau_{overflow}\right), \qquad (5)$$

The cavity exchanges with the surrounding by the orifice, the lateral wall and the back wall. The cavity thermal losses $\dot{Q}_{loss\_cavity}$ can be determined by:

$$\dot{Q}_{loss\_cavity} = \dot{Q}_{loss\_or} + \dot{Q}_{loss\_lateral\_wall} + \dot{Q}_{loss\_back\_wall}, \qquad (6)$$

$\dot{Q}_{loss\_lateral\_wall}$ and $\dot{Q}_{loss\_back\_wall}$ are calculated considering that radiative heat exchanges are negligible compared to convective ones from the insulating material surface. The convective heat exchange coefficient between the orifice and the surrounding is estimated from [17].

The two others cavity losses are determined using the various thermal resistances except the thermal resistance of contact between the cavity wall and the insulation which is neglected.

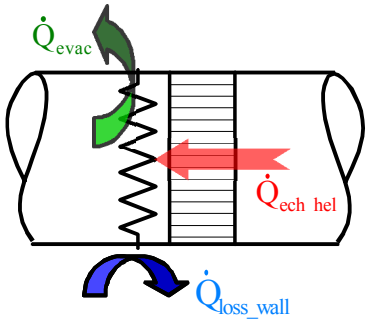

Fig. 7. Heat fluxes in the ambient and cold heat exchangers

The cold exchanger of the refrigerator as well as the heat exchangers at intermediate temperature, (Fig. 7) transfer on one side with the helium and on the other with a heat transfer fluid. The cold one is submitted to heat transfer with surroundings while such an exchange is neglected for the other ones because of the low temperature difference between these exchangers and ambient air. Applying the first law to the wall and to the heat transfer fluid of these elements gives:

$$\begin{cases} \dfrac{dU_{wall\_exch}}{dt} = \dot{Q}_{fluid-wall\_exch} + \dot{Q}_{hel-wall\_exch} + \dot{Q}_{loss\_exch} \\ \dfrac{dU_{fluid\_exch}}{dt} = \dot{Q}_{wall-fluid\_exch} + \dot{m}_{fluid\_exch}\left(h_{fluid\_input\_exch} - h_{fluid\_output\_exch}\right) + \dot{Q}_{visco\_exch} \end{cases}, \qquad (7)$$

The convective heat transfers between the heat exchanger walls and the fluids are given by:

$$\dot{Q}_{fluid-wall\_exch} = \alpha_{fluid-wall} \cdot A_{fluid-wall}\left(T_{fluid} - T_{wall\_exch}\right), \qquad (8)$$

Where the heat exchange coefficients ($\alpha_{fluid\text{-}wall}$) are calculated thanks to a correlation for a fluid flowing across a bank of tubes proposed in [18].

The viscous dissipation inside the exchanger is calculated by:

$$\dot{Q}_{visco\_exch} = \Delta P_{exch} \frac{\dot{m}_{fluid\_exch}}{\rho_{fluid}}, \quad (9)$$

Where ΔP_{exch} are the pressure drops inside the exchangers. They are calculated thanks to a correlation for a fluid flowing across a bank of tubes determined by [18] and ρ_{fluid} is the density of the fluid.

Each equation relative to the exchanger walls has a term of transfer with helium. A stationary model is used to determine these heat fluxes at each calculation time step of the quasi-stationary model [19].

3.3. The cool loop and cool thermal energy storage

The cool loop is mainly composed of flow pipes, an electrical load, a pump and a cool thermal storage.

3.3.1. Flow pipes

The flow pipes insure the connection between the elements. For this model, only the two longer pipes are considered (between the pump and the cold exchanger and between the cold exchanger and the cool storage). The temperatures of the fluid and the wall are assumed uniform inside the pipes. They are also considered perfectly insulated. The pipe walls are considered as an equivalent mass of fluid. With these hypotheses the energy balance on these elements is:

$$\frac{dU_{fluid+wall\_pipe}}{dt} = \dot{m}_{fluid\_cool\_circuit}\left(h_{fluid\_input\_pipe} - h_{fluid\_output\_pipe}\right) + \dot{Q}_{visco\_pipe}, \quad (10)$$

The viscous dissipations $\dot{Q}_{visco\_pipe}$, are calculated by (11) with the pressure drop determined by:

$$\Delta P_{pipe} = \rho_{fluid} \frac{V_{fluid}^{\ 2}}{2}\left[\sum K + \lambda \frac{L_{pipe}}{D_{int\_pipe}}\right], \quad (11)$$

With K the local coefficients of pressure drop for valves, changes of direction, …and λ the linear coefficient of pressure drop.

3.3.3. Circulating pump and electrical fluid circulation heater

We assumed that there is no variation of the internal energy of these elements. They are also considered adiabatic.

Applying the first law to the heat transfer fluid of these elements under these hypothesis gives:

$$\dot{Q}_{elec\_heater} = \dot{m}_{fluid\_cool\_circuit}\left(h_{fluid\_output\_heater} - h_{fluid\_input\_heater}\right), \quad (12)$$

Where $\dot{Q}_{elec\_heater}$ is the electrical power which feeds the heater.

A constant efficiency (η_{pump}) is considered for the pump. Considering these limitations, the energy balance of the fluid inside the circulating pump is expressed by:

$$h_{fluid\_output\_pump} - h_{fluid\_input\_pump} = \frac{\Delta P_{circuit}}{\rho_{fluid}}\left(1 - \eta_{pump}\right), \quad (13)$$

Where $\Delta P_{circuit}$ are the total pressure drops of the circuit.

3.3.3. The cool thermal energy storage

The model which has been already described in detail in a previous paper [20], considers the aspects of both the surrounding heat transfer fluid and the phase change material packed inside the

nodules in the charge mode as well as in the discharge mode. Only the main hypotheses and equations are presented here with a special adaptation to the selected configuration.

In order to simplify the physical model of the latent heat storage, the following assumptions were made:

- The tank is vertical with flow from the bottom to the top for the charge mode and the discharge mode;
- The flow in the tank is axial and incompressible;
- Variation of temperature of the heat transfer fluid occurs only along the axial direction, i.e. as checked experimentally [16], the temperature is independent of the radial position;
- The insulation of the tank is considered perfect;
- Heat transfer by conduction is neglected in the heat transfer fluid;
- Kinetic and potential energy changes are negligible;
- The tank is divided in several control volumes according to the height (Fig. 9);
- The nodules are considered as exchangers. The energy flux exchanged is proportional to the difference of temperature between the fluid and the interior of the spherical nodule;
- The supercooling phenomenon is taken into account.
- The variation of the internal energy of the tank elements (metal wall pipe, flow diffusers, etc..) is neglected.
- The pressure losses are considered for the flow inlet and outlet, the flow diffusers and the nodule bed thank to local coefficients of pressure drops.
-

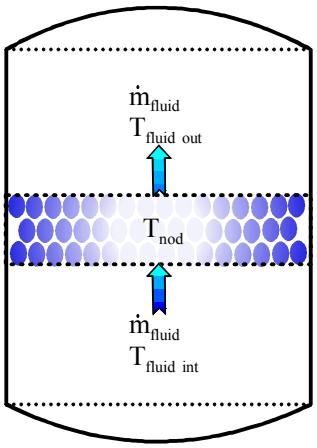

Fig. 9. Tank control volume.

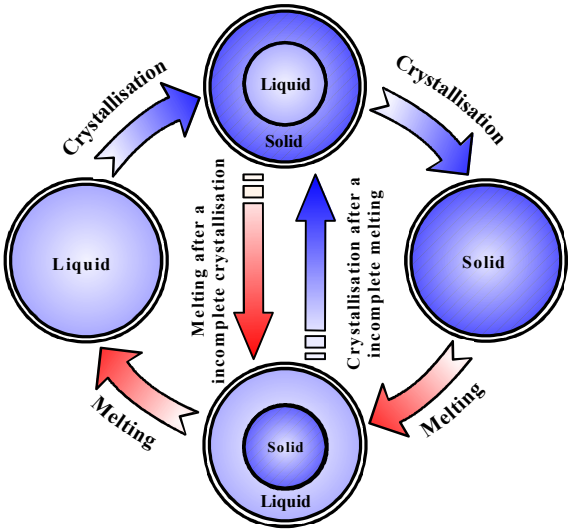

Fig. 10. State of nodule and way of crystallisation and melting

Based on these assumptions the energy balance equations in transient state in each control volume for the heat transfer fluid and each spherical nodule *i* are:

$$\frac{dU_{fluid}}{dt} = \dot{m}_{fluid}\left(h_{fluid\ in} - h_{fluid\ out}\right) + \sum_{i=1}^{N_{nod}} \dot{Q}_{nod-fluid,i} + \dot{Q}_{visco\_storage} \quad (14)$$

$$\frac{dU_{nod,i}}{dt} = m_{nod}\frac{du_{nod,i}}{dt} = \dot{Q}_{nod-fluid,i} \quad (15)$$

With

$$u_{nod,i} = \begin{cases} u_{ref} + Cv_{PCM\ solid}\left(T_{nod,i} - T_{ref}\right) & if \quad x_{nod,i} = 1 \\ u_{ref} + Cv_{PCM\ solid}\left(T_{melt} - T_{ref}\right) + x_{solid}\ L & if \quad 0 < x_{nod,i} < 1 \\ u_{ref} + Cv_{PCM\ solid}\left(T_{melt} - T_{ref}\right) + L + Cv_{PCM\ liq}\left(T_{nod,i} - T_{ref}\right) & if \quad x_{nod,i} = 0 \end{cases} \tag{16}$$

Even when the heat transfer fluid temperature is considered uniform in each layer, all the nodules of each layer do not simultaneously pass through the phase change at the melting temperature T_{melt} during cooling because of the supercooling and the erratic character of the crystallisation. The nodules can be in different states (non-crystallised, entirely crystallised or partly crystallised) according to their own value of the beginning of the crystallization (Fig. 10).

Applying the nucleation laws, the number of new crystallisations and the corresponding fluxes can be calculated at each time t [20].

Considering a nodule of inner radius r_{int} (Fig. 11). Uniform cooling of its surface will result in a spherically symmetric crystallisation-front, $r = r_{interface}(t)$ the inner radius of solid PCM, propagating inwards from $r = r_{int}$ with liquid at T_{melt} for $0 \le r \le r_{interface}(t)$ and solid for $r_{interface}(t) \le r \le r_{int}$. Assuming constant thermal properties in each phase, the steady-state solution of the heat conduction in the solid phase has the form (θ is the temperature of the solid PCM):

$$\theta(r,t) = T_{melt} + \left[T_{fluid}(t) - T_{melt}\right] \frac{1 - \dfrac{r_{interface}(t)}{r}}{\left(\dfrac{k_{PCMsolid}}{k_{env}} - 1\right)\dfrac{r_{interface}(t)}{r_{\text{int}}} + \left(\dfrac{k_{PCMsolid}}{\alpha_{ext} r_{ext}} - \dfrac{k_{PCMsolid}}{k_{env}}\right)\dfrac{r_{interface}}{r_{ext}} + 1} \tag{17}$$

The interface conditions here have the standard form:

$$k_{PCMsolid}\left[\frac{\partial\theta(r,t)}{\partial r}\right]_{r=r_{interface}(t)} = \frac{-\dot{Q}_{nod-fluid,i}}{4\pi r_{interface}^2(t)} \tag{18}$$

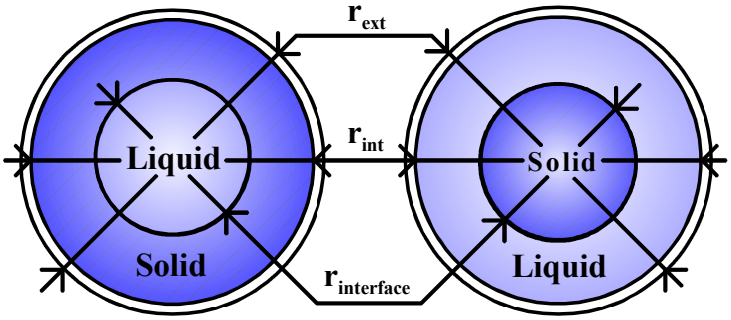

Fig. 11. Crystallization inside a nodule (left) and melting inside the nodule (right).

The determination of $\dot{Q}_{nod-fluid}$ before crystallisation starts and after crystallisation is finished is done considering the uniform PCM temperature and it is possible to write that the internal energy variation in the PCM is equal to the flux that leaves the nodule.

The heat transfer coefficient between the nodule and the fluid is determined by a correlation [20] and so depends on the flow rate and on the fluid temperature.

Supercooling occurs only upon crystallisation but never upon melting. So, all the nodules from each layer simultaneously pass through the phase change at the melting temperature T_{melt}.

According to a simplifying assumption, the melting-front is considered to be concentric (Fig. 11) and equations for $\dot{Q}_{nod-fluid}$ are the same than for crystallisation. During the melting process, heat is transfered by natural convection and conduction. Only the heat conduction equation is kept into consideration but an apparent thermal conductivity [21] is used in order to take the natural convection into account.

4. Results

From the model described in the previous section, numerical simulations of the experimental plant have been carried out assuming a constant ambient temperature of 20°C. The solar radiation conditions that have been used are the DNI measured between the 1st and the 7th of July 2006 by PROMES laboratory at Odeillo (South of France) (Fig. 12). The main parameters that have been considered for this simulation are summarised in Table 1.

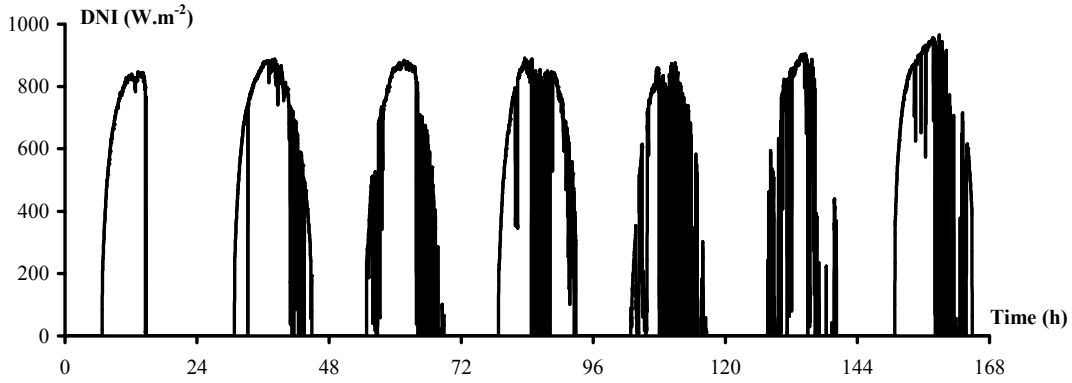

Fig 12. DNI

Table 1. Main simulation parameters

Solar concentrator aperture area (m²)	13.5	Hot heat exchanger mass (kg)	30
Shadow area on the concentrator (m²)	3.5	Ambient heat exchanger mass (kg)	1
Reflectivity of the concentrator	0.92	Cold heat exchanger mass (kg)	1
Cavity orifice diameter (m)	0.1	Electrical power of the heater (W)	350
Solar overflow rate	0.1	MCP nodule diameter (mm)	77

4.1. Standard case

A standard case for design and operating parameter of the cool storage has been considered (Table 2). The simulation results of this case are presented in this section.

Table 2. Main storage tank design and operative parameters

	Standard case	Variation for parametric study
Tank volume (m^3)	0.2	0.15 and 0.25
Masse flow rate ($kg.s^{-1}$)	0.1	0.05 and 0.2
PCM melting temperature (°C)	-21.3	-18.8 and -26.2

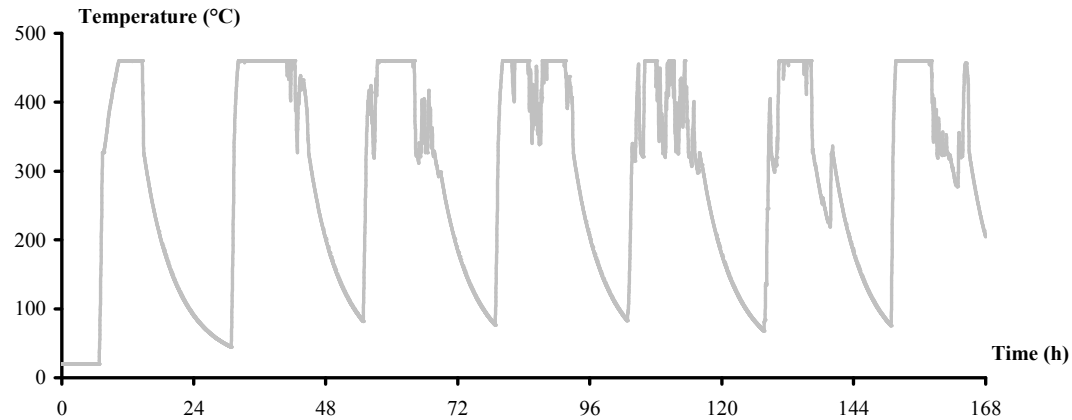

Fig 13. Temperature of the hot exchanger of the generator

As shown in Fig. 13, when the sun is shining, the temperature of the hot exchanger of the generator increases extremely rapidly to reach the temperature threshold for wave generation. Actually the machine starts only if a sufficient temperature gradient exists between the two heat exchangers of the engine cycle. According to previous experiences, the starting hot temperature (and also stop temperature when the exchanger temperature decreases) of the generator has been set at 600 K. The solar power available is very large compared to the one consumed by the acoustic wave generation and the thermal losses so that the temperature of the hot exchanger continues to grow rapidly to reach the regulating temperature. This regulation is ensured by the control of the absorbed solar radiation thank to the solar flux modulator. When the DNI is important, it can shut up to 45% of the reflected solar power. At the end of the day or during cloudy periods, the hot exchanger is cooled due to the power consumed by the acoustic wave generation (if its temperature is higher than 600 K) and due to the radiative and convective heat losses. The hot exchanger behaviour is roughly the same for each simulated days with variations in function of the solar radiation fluctuations.

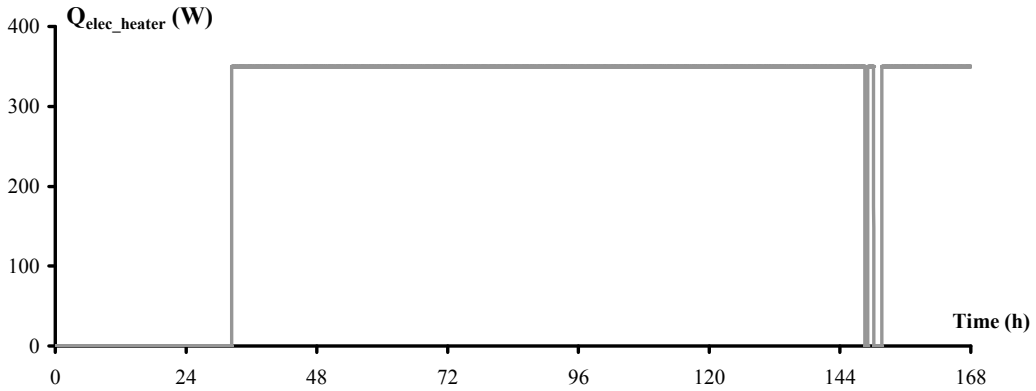

Fig 14. Electrical power of the fluid heater

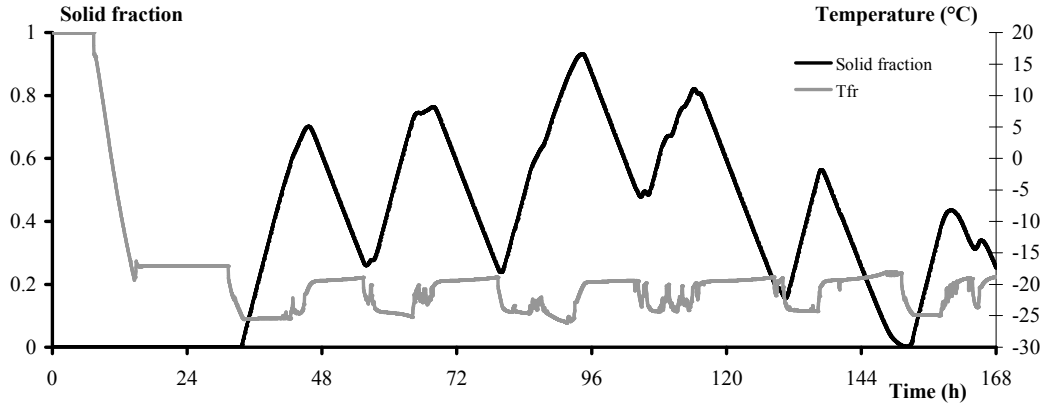

Fig 15. Solid fraction in the storage tank and temperature of the cold exchanger of the refrigerator

The operative conditions corresponding to the frigorific loads have been set as follows: a constant heating power if the fluid temperature at its outlet stays lower than -18°C and no heating power if this temperature is higher than this limit. To ensure the cooldown of the storage and the loop elements the heater is turned off during the first 30 hours (Fig. 14 and 15). During this period, when the refrigerator works, the temperature of the cold exchanger of the refrigerator decreases to reach a temperature close to the melting temperature of the PCM (Fig. 15). Due to the adiabatic assumption and no heating power, the temperature of the storage remains constant during the first night. At the beginning of the second day (close to 32 hours after the beginning of the simulated experimentation) the tank temperature continues to decrease below the melting temperature of the

PCM. Due to thermal resistances between the fluid and the nodule and due to the supercooling effect, the temperature of the fluid has to be a few degrees lower than the melting temperature to initiate the crystallisation. Even if the refrigerator continues to produce a frigorific power, the temperature of the cold exchanger remains quasi constant after the initiation of the crystallisation thank to the isothermal behaviour of the nodules during this phase. At the end of the second day, the majority of the PCM is solid. During the following night, a large part of the solid PCM is melting to supply the loads. During the next four days, the system reaches a quasi periodically steady state condition, the storage tank solid fraction evolves between the same levels from one day to the other and the temperature of the cold loop stays close to the melting temperature of PCM. Due to a low insolation during the two last days, the solid fraction of the tank decreases and there are periods where the storage cannot provide the cooling capacity within the imposed temperature condition.

4.2. Parametric study

From the standard case described previously, we consider the effects of the variation of the principal parameters of the cold thermal energy storage on the temperature of this storage and on the global performance of the experimental plant. The effect of the supercooling is firstly analyzed. Then the effect of the storage tank volume, the melting temperature of the PCM and the fluid mass flow rate, are successively considered (Table 2).

Supercooling effect: A simulation has been made considering no supercooling effect. As expected the lack of supercooling allows the initiation of crystallization of the PCM at a temperature higher than when this effect is considered. This temperature difference can be observed (Fig. 16) during the first crystallization stage. During the next four days, no difference can be observed because a large number of nodules remain constantly partially crystallized. Because of the total discharge of the stock during the night preceding, this phenomenon is again perceptible on the last day.

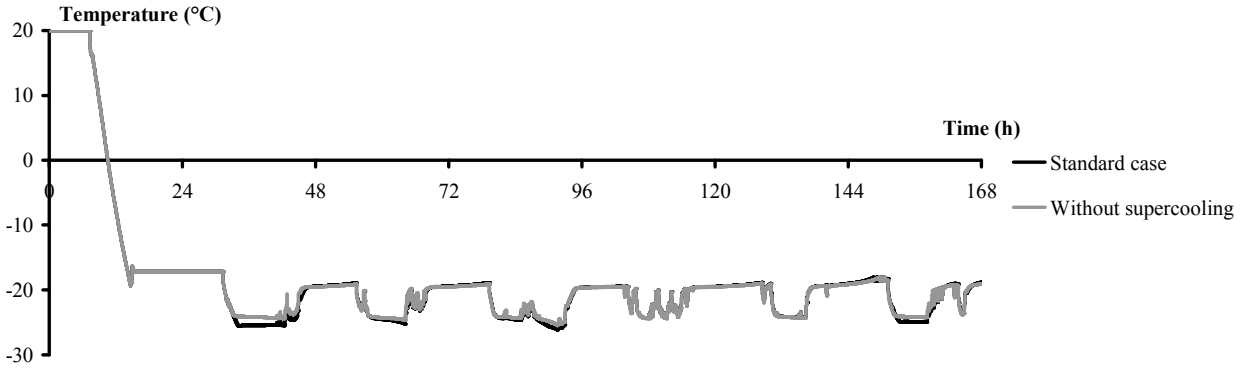

Fig. 16. Temperature of the cold exchanger of the refrigerator with and without PCM supercooling

Volume of the storage tank: The variations of the tank volume have significant impact on the cold exchanger temperature (Fig 17) and the PCM solid fraction (Fig 18). With the smallest tank there are periods where all the PCM into the tank is solid, thus the residual energy have to be stored as sensible heat. This generates very low temperatures in the cold circuit. Considering the largest tank, due to higher mass of fluid and PCM, a larger part of the energy is stored as sensible heat. The solid fractions are thus in this case lower than the other one. Due to this, with this configuration, there is a large period of time between the two last days where the storage cannot provide the cooling capacity.

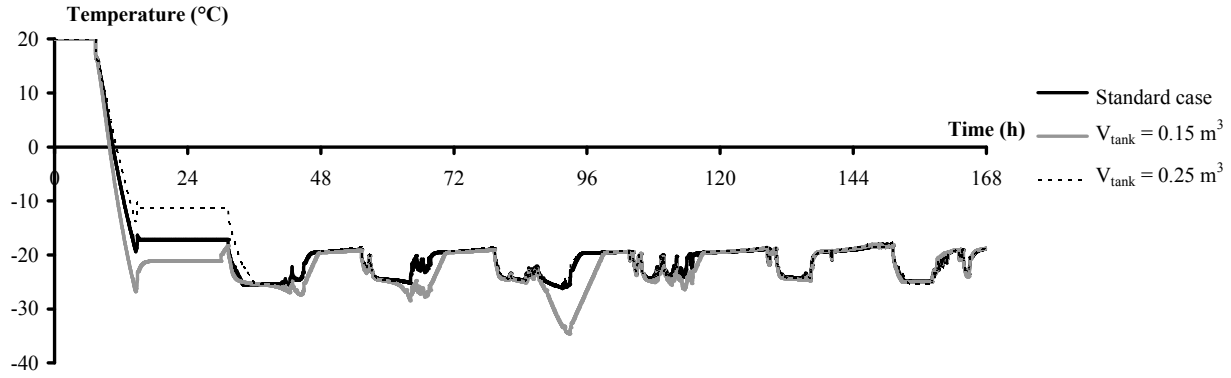

Fig. 17. Temperature of the cold exchanger of the refrigerator for different tank volumes

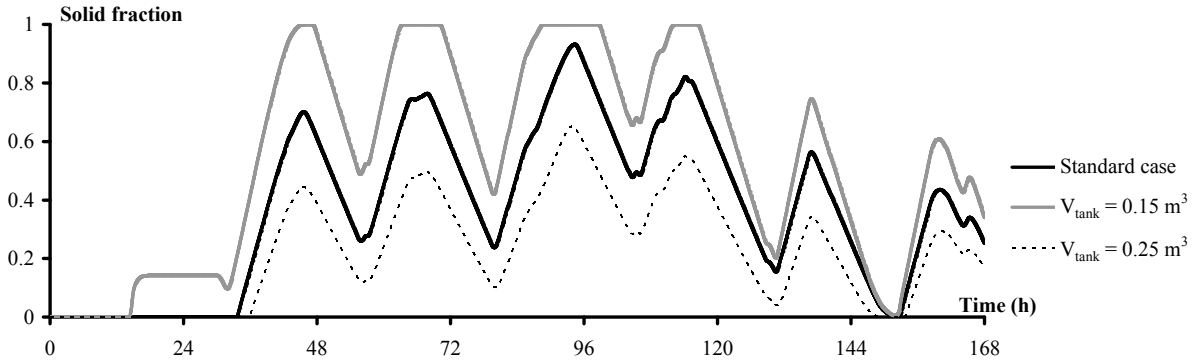

Fig. 18. Solid fraction in the storage tank for different tank volumes

Heat transfer fluid mass flow rate: Simulations have been made for different heat transfer fluid mass flow rates. The obtained results show that in the simulation conditions, this parameter has only a slight effect on the operation of the cold circuit (Fig. 19).

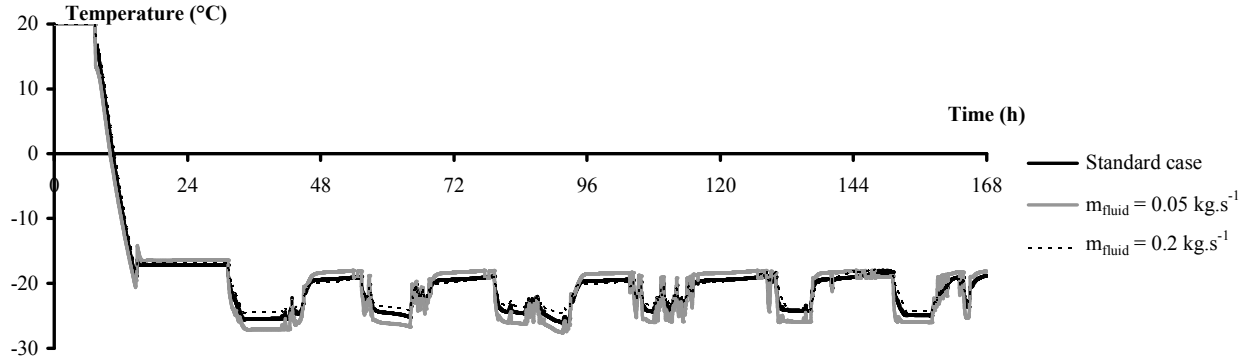

Fig 19. Temperature of the cold exchanger of the refrigerator for different mass flow rates

Melting temperature of the PCM: For these simulations the thermophysical properties of the PCM (except the melting temperature) are considered identical. Because of the low temperature difference between the expected temperature at the heater and the melting temperature of the highest PCM melting temperature, the major part of the energy is stored as sensible heat (Fig. 20. and Fig. 21). Due to the difficulty of the refrigerator to reach a low temperature to initiate the crystallisation of the lowest melting temperature PCM, the variation of the solid fraction in this case is low. In these two cases the temperature stabilisation which is expected with latent energy storage is not assured (Fig 21).

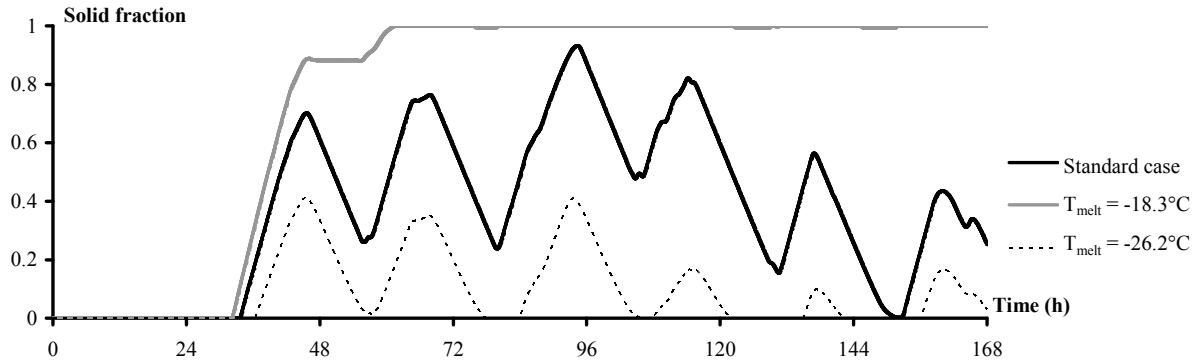

Fig 20. Solid fraction in the storage tank for different PCM melting temperatures

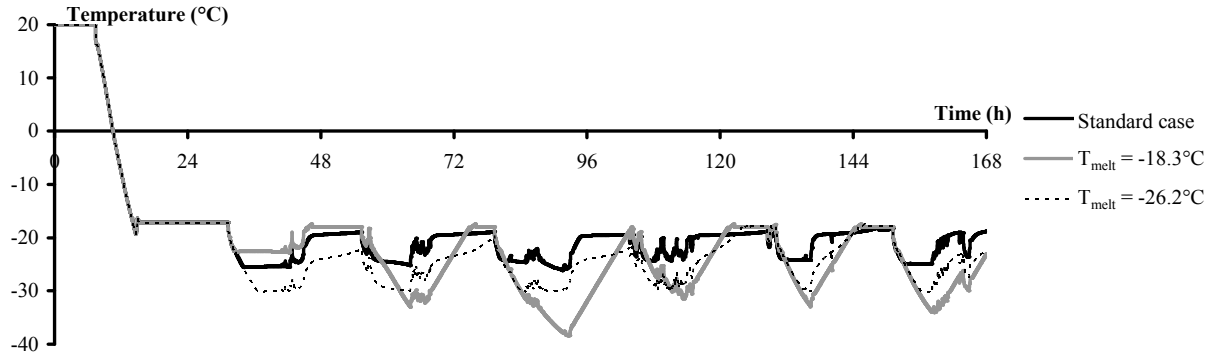

Fig 21. Temperature of the cold exchanger of the refrigerator for different PCM melting temperatures

4. Conclusion

A solar driven thermoacoustic cooler which consists of a thermoacoustic engine that converts solar energy into acoustic waves, coupled to a thermoacoustic cooler that converts this acoustic energy into cooling effect, has been studied using a numerical model. The designed prototype would be able to deliver a refrigerating capacity of about 1 kW at -30°C.

In order to guarantee a sufficient cooling capacity to face to refrigeration loads in spite of the production fluctuations, a cold storage using encapsulated PCM has been considered. It stores the excess cooling power when the sun is highly shining and restitutes it at night or during cloudy hours.

The developed model permits to determine the future performances of the prototype but also to choose the best configuration of the storage tank which has to be adapted to the loads. The main design parameters for the cool storage are the tank volume, the crystallization and melting temperature of the PCM and the mass flow rate of the heat transfer fluid.

Acknowledgments

This work was carried out within the framework of the TACSOL project. It is funded by the ANR PRECODD. We would like to thank our project partners, S. Cordillet (PROMES), P. Duthil (IPNO), M.X. François (Hekyom), T. Le Polles (Hekyom), G. Olalde (PROMES), M. Pierens (IPNO), J.P. Thermeau (IPNO), for their help.

Nomenclature

A area, m²

C specific heat, J kg^{-1} K^{-1}

DNI Direct Normal Irradiation, W m^{-2}

h enthalpy, J kg^{-1}

k thermal conductivity, W m^{-1} K^{-1}

K local coefficient of pressure drop

L length, m

L latent heat of the PCM, J kg^{-1}

$\dot{m}$ mass flow rate, kg s^{-1}

N number of nodules in the tank layer

ΔP pressure drop, Pa

$\dot{Q}$ heat flux, W

r radius, m

t time, s

T temperature, K

u specific internal energy, J kg^{-1}

U internal energy, J

x solid fraction of PCM

Greek symbols

α *convective* heat transfer coefficient, W m^{-2} K^{-1}

ε *emissivity*

χ reflectivity of the concentrator

λ linear coefficient of pressure drop

ρ density, kg m^{-3}

σ Stefan–Boltzmann constant, W m^{-2} K^{-4}

τ rate

η efficiency

Subscripts and superscripts

abs absorbed

amb ambient

collect collected

collector solar collector

env nodules envelope

exch exchanger

ext external

fluid heat transfer fluid

hg hot exchanger of the generator

hel-wall exchange between the helium and the exchanger wall

int internal

interface interface liquid/solid of the PCM

liq liquid phase of the PCM

loss yhermal losses

melt melting of the PCM

modul modulated or solar flux modulator

nod nodule
or orifice
PCM Phase Change Material
ref reference
reflect reflected
sol solar
solid solid phase of the PCM
visco viscous

References

[1] J. M. Calm, « Emissions and environmental impacts from air-conditioning and refrigeration systems », International Journal of Refrigeration 2002; 25 (3): 293-305.

[2] C. James M., « The next generation of refrigerants – Historical review, considerations, and outlook », International Journal of Refrigeration 2008; 31(7): 1123-1133.

[3] D. S. Kim et C. A. Infante Ferreira, « Solar refrigeration options - a state-of-the-art review », International Journal of Refrigeration 2008;31(1): 3-15.

[4] F. Zink, J. S. Vipperman, et L. A. Schaefer, « Environmental motivation to switch to thermoacoustic refrigeration », Applied Thermal Engineering 2010; 30(2–3): 119-126.

[5] J. J. Wollan, G. W. Swift, S. Backhaus, et D. L. Gardner, « Development of a thermoacoustic natural gas liquefier », presented at the AIChE New Orleans Meeting, New Orleans, 2002.

[6] G. Yu, E. Luo, et W. Dai, « Advances in a 300 Hz thermoacoustic cooler system working within liquid nitrogen temperature range », Cryogenics, vol. 50, n°. 8, p. 472-475, Aug. 2010.

[7] J. Y. Hu, E. C. Luo, S. F. Li, B. Yu, et W. Dai, « Heat-driven thermoacoustic cryocooler operating at liquid hydrogen temperature with a unique coupler », Journal of Applied Physics, vol. 103, p. 104906, 2008.

[8] M. E. Poese, R. W. M. Smith, S. L. Garrett, R. van Gerwen, et P. Gosselin, « Thermoacoustic refrigeration for ice cream sales », in Proceedings of 6th IIR Gustav Lorentzen Conference, Glasgow, UK, 2004.

[9] J. A. Adeff et T. J. Hofler, « Design and construction of a solar-powdered, thermoacoustically driven, thermoacoustic refrigerator », The Journal of the Acoustical Society of America, vol. 107, n°. 6, p. L37-L42, 2000.

[10] C. Shen, Y. He, Y. Li, H. Ke, D. Zhang, et Y. Liu, « Performance of solar powered thermoacoustic engine at different tilted angles », Applied Thermal Engineering, vol. 29, n°. 13, p. 2745-2756, Sept. 2009.

[11] A. Sharma, V. V. Tyagi, C. R. Chen, et D. Buddhi, « Review on thermal energy storage with phase change materials and applications », Renewable and Sustainable Energy Reviews, vol. 13, n°. 2, p. 318-345, Febr. 2009.

[12] F. Nepveu, A. Ferrière, et F. Bataille, « Thermal model of a dish/Stirling systems », Solar Energy, n°. 83, p. 81-89, 2009.

[13] S. Cordillet, P. Duthil, F. Nepveu, T. Le Polles, G. Olalde, A. Salome, et J.-P. Thermeau, « Theoretical proof of concept of an optimal solar receiver to produce low-temperature (-40°C) cooling using a thermoacoustic tri-thermal machine », in Proceedings of SolarPACES 2010, Perpignan, 2010.

[14] S. Cordillet, P. Duthil, E. Guillot, G. Olalde, et C. Gueymard, « Potential effects of rapid incident flux variations on the design of a solar thermoacoustic receiver », in Proceedings of SolarPACES 2010, Perpignan, 2010.

[15] G. Swift et Acoustical Society of America., Thermoacoustics: a unifying perspective for some engines and refrigerators. Melville NY: Acoustical Society of America through the American Institute of Physics, 2002.

[16] J. P. Bédécarrats, J. Castaing-Lasvignottes, F. Strub, et J. P. Dumas, « Study of a phase change energy storage using spherical capsules. Part I: Experimental results », Energy Conversion and Management, vol. 50, n°. 10, 2527-2536, oct. 2009.
[17] F. Nepveu, « Production décentralisée d'électricité et de chaleur par système Parabole/Stirling: Application au système EURODISH », Université de Perpignan, Odeillo, France, 2008.
[18] Y. A. Çengel, Heat transfer: a practical approach. Boston: McGraw-Hill, 2003.
[19] M. Perier-Muzet, J. Castaing-Lasvignottes, P. Stouffs, P. Duthil, J.-P. Thermeau, G. Olalde, S. Cordillet, et M.-X. François, Modélisation et simulation transitoire d'un refrigerateur thermoacoustique, in Actes Congrès Français de Thermique 2010, Le Touquet, (2): 851-856.
[20] J. P. Bédécarrats, J. Castaing-Lasvignottes, F. Strub, et J. P. Dumas, « Study of a phase change energy storage using spherical capsules. Part II: Numerical modelling », Energy Conversion and Management, vol. 50, n°. 10, p. 2537-2546, Oct. 2009.
[21] S. Fukusako et M. Yamada, « Recent advances in research on melting heat transfer problems », presented at the 10th Int Heat Transfer Conf, Brighton, Brighton, 1994, 313-331.